



HAL
open science

Reversible colossal barocaloric effects near room temperature in 1-X-adamantane (X=Cl, Br) plastic crystals

Araceli Aznar, Philippe Négrier, Antoni Planes, Lluís Mañosa, Enric Stern-Taulats, Xavier Moya, María Barrio, Josep-Lluís Tamarit, Pol Lloveras

► **To cite this version:**

Araceli Aznar, Philippe Négrier, Antoni Planes, Lluís Mañosa, Enric Stern-Taulats, et al.. Reversible colossal barocaloric effects near room temperature in 1-X-adamantane (X=Cl, Br) plastic crystals. *Applied Materials Today*, 2021, 23, pp.101023. 10.1016/j.apmt.2021.101023 . hal-03261805

HAL Id: hal-03261805

<https://hal.science/hal-03261805>

Submitted on 16 Jun 2021

HAL is a multi-disciplinary open access archive for the deposit and dissemination of scientific research documents, whether they are published or not. The documents may come from teaching and research institutions in France or abroad, or from public or private research centers.

L'archive ouverte pluridisciplinaire **HAL**, est destinée au dépôt et à la diffusion de documents scientifiques de niveau recherche, publiés ou non, émanant des établissements d'enseignement et de recherche français ou étrangers, des laboratoires publics ou privés.

Reversible colossal barocaloric effects near room temperature in 1-X-adamantane (X=Cl, Br) plastic crystals

Araceli Aznar,¹ Philippe Negrier,² Antoni Planes,³ Lluís Mañosa,³ Enric Stern-Taulats,⁴ Xavier Moya,⁴ María Barrio,¹ Josep-Lluís Tamarit,¹ Pol Lloveras^{1,*}

¹Grup de Caracterizació de Materials, Departament de Física, EEBE and Barcelona Research Center in Multiscale Science and Engineering, Universitat Politècnica de Catalunya, Eduard Maristany, 10-14, 08019 Barcelona, Catalonia

²Université de Bordeaux, LOMA, UMR 5798, F-33400 Talence, France

³Departament de Física de la Matèria Condensada, Facultat de Física, Universitat de Barcelona, Martí i Franquès 1, 08028 Barcelona, Catalonia

⁴Department of Materials Science, University of Cambridge, Cambridge, CB3 0FS, UK
*email: pol.lloveras@upc.edu

Plastic crystals undergo phase transitions with unusually large volume and entropy changes related to strong molecular orientational disordering. These features have led to a resurgent interest in these materials because recently they have shown great potential in solid-state cooling applications driven by pressure. Here we demonstrate that two plastic crystals derived from adamantane -1-Br-adamantane and 1-Cl-adamantane- undergo colossal reversible barocaloric effects under moderate pressure changes in a wide temperature span near room temperature thanks to a relatively small hysteresis and very high sensitivity of the transition temperature to pressure. In particular, 1-Cl-adamantane displays an optimal operational temperature range covering from ~40 K below and up to room temperature, and under a pressure change of 1 kbar this compound outperforms any other barocaloric material known so far. Our work gives strong support to plastic crystals as best candidates for barocaloric cooling. We also provide insight into the physical origin of the entropy changes through the analysis of the disorder on the involved phases.

Keywords: Barocaloric effects, plastic crystals, 1-bromoadamantane, 1-chloroadamantane, pressure, entropy

1. Introduction

One of the numerous urgent environmental challenges posed by the global warming is related to the need to replace the widely extended use of vapor compression in billions of air conditioners and refrigerators [1,2]. This mature technology shows moderate efficiencies and uses greenhouse fluids that contribute significantly in terms of CO₂-equivalent emissions. One of the best-positioned alternative methods is based on the exchange of the latent heat at solid-state first-order phase transitions driven by external

fields such as magnetic, electric or mechanic, leading to magnetocaloric, electrocaloric and mechanocaloric effects, respectively [3-5]. In addition to the use of Global Warming Potential-free refrigerants, these methods may also exhibit additional advantages as higher efficiencies or scalability, allowing other applications such as wearables, solutions for the overheating of electronic elements that restrict their miniaturization, or for heat pumping [6] and energy harvesting and conversion. In the last years, intense research has led to significant advances as for magnetocaloric (MC), electrocaloric (EC) and elastocaloric (eC) materials and prototypes [7]. However, a major limitation for a competitive implementation is given by the available nontoxic materials, which exhibit small refrigerant capacity and may suffer from irreversibility. These issues may be overcome by applying high fields, but this is technologically challenging, energetically costly and may be destructive, leading to mechanical failure and/or dielectric breakdown. Pressure-induced (barocaloric, BC) effects have been less investigated but on the one hand they promise better efficiencies than vapor compression [8] and on the other hand the abundance of potential BC materials [9] has allowed the identification of BC effects that surpass in many aspects best MC, EC and eC effects reported so far.

Recently, plastic crystals have been identified as outstanding barocaloric (BC) agents [10-12] because they may display enormous entropy changes related to orientational disorder released across solid-to-solid phase transitions that are sensitive to mechanical stress due to associated large volume changes. In the case of plastic crystal neopentylglycol, it has been shown that, at the atomic scale, a large compressibility facilitates the shortening of the hydrogen bond length by application of pressure, thus leading to an increase of the orientational energy barrier and, therefore, to the stabilization of the ordered phase [13].

While the extremely high fragility of these compounds prevents the cyclic application of uniaxial stress without compromising their mechanical integrity and hinders very much the application of electric fields on their polar molecules, in form of powder plastic crystals can be easily subjected to changes in hydrostatic pressure. Therefore, these compounds may offer opportunities in energy-related applications based on controlling by pressure the absorption and release of large amounts of latent heat associated with their solid-state transitions, such as the mentioned BC effects for cooling or heat pumping.

To date, among plastic crystals only neopentane derivatives [10-12] and C₆₀ [14] have been analyzed for BC applications and so there are still many compounds of this kind that remain unexplored. In this work we open up the BC analysis to two plastic crystals derived from adamantane (C₁₀H₁₆): 1-bromoadamantane (C₁₀H₁₅Br, 1-Br-ada for short) and 1-chloroadamantane (C₁₀H₁₅Cl, 1-Cl-ada for short). 1-Br-ada and 1-Cl-ada are obtained via substitution of an H atom linked to a 3-coordinated carbon site by a Br or Cl atom, respectively [15]. They are widely used as precursors in the synthesis of other adamantane derivatives used in pharmaceutical industry as antiviral drugs and also for the synthesis of polymers and other materials [16,17]. At low temperatures both 1-Br-ada and 1-Cl-ada are isostructural and exhibit a fully ordered monoclinic (M) structure (*P*2₁/*c*, *Z*=4) [18]. At high temperatures, they are also isostructural, arranging in an FCC lattice (*Fm* $\bar{3}$ *m*, *Z*=4) with orientational disorder that has been suggested to consist of quasi-free rotation [19]. In 1-Cl-ada, the orientational disorder fully develops in a single M→FCC transition that displays a giant entropy change $\Delta S_{M \rightarrow FCC} = 135 \text{ J K}^{-1} \text{ kg}^{-1}$ and volume change $\Delta V_{M \rightarrow FCC} \sim 47 \cdot 10^{-6} \text{ m}^3 \text{ kg}^{-1}$ (corresponding to a relative volume change $\frac{\Delta V_{M \rightarrow FCC}}{V_M} \sim 6\%$). These two quantities entail a sensitivity of the transition temperature to

pressure $\frac{dT_{M \rightarrow FCC}}{dp} \sim 27 \text{ K kbar}^{-1}$. Differently, in 1-Br-ada the orientational disorder arises across two transitions $M \rightarrow O \rightarrow FCC$, where O refers to an intermediate semioordered orthorhombic phase (Pmcn, Z=4). In this phase, disorder is believed to consist of a 6-fold molecular rotation about the three-fold molecular axis C_{3v} [19]. Although both $M \rightarrow O$ and $O \rightarrow FCC$ transitions take place close to each other near room temperature, only the $O \rightarrow FCC$ raises interest for BC cooling applications as it involves by far most of the total entropy change associated with full orientational disorder and a much larger transition volume change. In particular, $\Delta S_{M \rightarrow O} \sim 21 \text{ J K}^{-1} \text{ kg}^{-1}$ and $\Delta V_{M \rightarrow O} \sim 6 \cdot 10^{-6} \text{ m}^3 \text{ kg}^{-1}$ ($\frac{\Delta V_{M \rightarrow O}}{V_M} \sim 0.9\%$) whereas $\Delta S_{O \rightarrow FCC} \sim 107 \text{ J K}^{-1} \text{ kg}^{-1}$ and $\Delta V_{O \rightarrow FCC} \sim 40 \cdot 10^{-6} \text{ m}^3 \text{ kg}^{-1}$ ($\frac{\Delta V_{O \rightarrow FCC}}{V_O} \sim 6\%$). In turn, the values for the $O \rightarrow FCC$ transition yield $\frac{dT_{O \rightarrow FCC}}{dp} \sim 33.6 \text{ K kbar}^{-1}$. These giant values from literature for the transition entropy change and dT/dp at the $M \rightarrow FCC$ transition for 1-Cl-ada and at the $O \rightarrow FCC$ transition for 1-Br-ada suggest an excellent BC potential for these two transitions, but the transition hysteresis and high-pressure transition properties in and out of thermodynamic equilibrium, which remain unknown, could confute this supposition. In this work we study these features and find colossal BC effects well above a hundred $\text{J K}^{-1} \text{ kg}^{-1}$ for the two transitions, that are reversible at moderate pressures and span over few tens of K near room temperature. We also calculate the refrigerant capacity and the coefficient of refrigerant performance, confirming the great potential of these materials in pressure-driven heat exchange. Our method combines variable-pressure quasi-direct isobaric heat flow measurements across the temperature-induced transition and indirect estimation of thermal expansion-related BC effects from x-ray measurements. We also report the unknown structure of the O phase of 1-Br-ada, that confirms its partial orientational disorder.

2. Experimental details

Powdered samples of 1-Br-ada (99 wt% purity) and 1-Cl-ada (98 wt%) were purchased from Sigma-Aldrich and used as received. Experimental details of high-resolution X-ray powder diffraction measurements can be found in Ref. [15]. Molecular energy minimization with the Forcite module using the Dreiding forcefield available in Materials Studio Program [20] has been used to build up a rigid body molecule. It is well-known that molecular parameters of adamantane derivatives, in particular those consisting in 1-X- or 2-X-adamantane derivatives, are virtually the same [21-27]. For the final structural solution, rigid molecules were placed in a randomly oriented general position and through Powder Solve using Monte-Carlo approach, both the position and orientation of molecules within the unit lattice were refined. The ultimate structural solution was obtained by means of Rietveld refinement [28], in which the position and orientation of the molecule, within the rigid-body constraint, with a single overall isotropic displacement parameter and the preferred orientation (using the Rietveld-Toraya function [29]) were refined. The obtained R factors were $R_{wp} = 8.11\%$, $R_p = 5.61\%$ for the O phase of 1-Br-ada. To ensure the robustness of the structural refinement of the orthorhombic phase we have applied the same method and experimental conditions to the low-temperature monoclinic phase, previously reported from a study of single-crystal X-ray diffraction [18]. By doing so, the obtained structure for this monoclinic phase is virtually the same and the aforementioned quality factors being $R_{wp} = 8.53\%$, $R_p = 6.18\%$, very close to those of the O phase.

Calorimetry at normal pressure was carried out using a conventional Differential Scanning Calorimeter Q100 from TA Instruments. Pressure-dependent differential thermal analysis was performed using two homemade high-pressure cells that operate in a pressure range up to 3 kbar and use Bridgman K-type thermocouples (chromel-alumel, ± 2.2 K of tolerance, from Pyromation) as thermal sensors for both temperature and heat flow measurements. For 1-Br-ada, the used cell works within a temperature range from room-temperature to 473 K controlled by a resistive heater. Heating ramps were carried out at 3 K min^{-1} and coolings were performed with an air stream system at an average rate of $\sim 2.5 \text{ K min}^{-1}$. For 1-Cl-ada the used cell works within a temperature range from 200 K to 393 K controlled by an external thermal bath (Lauda Proline 1290). Heating and cooling ramps were performed at $\sim 4 \text{ K min}^{-1}$ and $\sim 2 \text{ K min}^{-1}$, respectively. A Pt-100 thermometer (RS components; accuracy $\pm 0.30 \text{ K}$ at 273.15 K , ± 0.80 at 373.15 K) was used to monitor the temperature ramps by means of a temperature controller. In both cells, few hundreds of mg of each sample were encapsulated in tin capsules along with a perfluorinated inert fluid (Galden Bioblock Scientist) to remove air. It was checked that this fluid does not affect the thermodynamic transition properties of the sample. A hole was drilled in the tin capsules to insert the Bridgman thermocouples. The pressure-transmitting fluid used in the pressure circuit was DW-Therm M90.200.02 (Huber). A high-pressure transducer Model HP from Honeywell (range 0-5.2 kbar, 0.5% accuracy) was used as pressure sensor. A manual pressure pump was used to change pressure. Calorimetric signals were recorded under nearly isobaric conditions using a custom-built software.

3. Results and discussion

3.1 Characterization of the phase transitions

Figure 1a shows the Rietveld refinement of the 1-Br-ada O phase in which all H atoms and all but one C atom exhibit an occupancy of 50%, due to $\frac{\pi}{3}$ rotations about the C-Br three-fold axis (cif number: CCDC 2042237). Unit cell representations of the O cell are displayed in Figs 1b,c projected onto the (010) and (100) planes, respectively. Since this disorder leads to $N_O = 2$ possible molecular configurations and the M phase is completely ordered, the contribution to the $M \rightarrow O$ transition entropy change due to the increase in the molecular configurations is $\Delta S_{M \rightarrow O}^c = RM^{-1} \ln(N_O/N_M) = RM^{-1} \ln 2 \sim 27 \text{ J K}^{-1} \text{ kg}^{-1}$. This value is of the order of the aforementioned total transition entropy change $\Delta S_{M \rightarrow O} \sim 21 \text{ J K}^{-1} \text{ kg}^{-1}$ [15], which indicates that there are no other significant contributions to the latter, such as the entropic contribution concerning the volume change.

Calorimetry measurements at constant pressure, as shown in Fig. 2a for 1-Cl-ada and Fig. 2b for 1-Br-ada, yielded positive and negative $\frac{dQ}{dT} \equiv d\dot{Q}/|d\dot{T}|$ peaks in temperature corresponding to endothermic and exothermic phase transitions, respectively. Transition enthalpy changes $\Delta H_{II \rightarrow I}$ and $\Delta H_{I \rightarrow II}$, and transition entropy changes $\Delta S_{II \rightarrow I}$ and $\Delta S_{I \rightarrow II}$, were determined from integrations in T of $dQ/|dT|$ and of $\left(\frac{1}{T}\right) \frac{dQ}{|dT|}$ peaks after baseline subtraction, respectively. Here, II stands for the M phase for 1-Cl-ada and for the O phase for 1-Br-ada, whereas I stands for the FCC phase for the two compounds. At atmospheric pressure, for 1-Cl-ada we found $\Delta H_{II \rightarrow I} = 32 \pm 1 \text{ kJ kg}^{-1}$, $\Delta H_{I \rightarrow II} = 31.5 \pm 1.0 \text{ kJ kg}^{-1}$, $\Delta S_{II \rightarrow I} = 132 \pm 4 \text{ J K}^{-1} \text{ kg}^{-1}$ and $\Delta S_{I \rightarrow II} = 136 \pm 4 \text{ J K}^{-1} \text{ kg}^{-1}$ whereas for 1-Br-ada, we

found $\Delta H_{II \rightarrow I} = 32 \pm 1 \text{ kJ kg}^{-1}$, $\Delta H_{I \rightarrow II} = 31 \pm 1 \text{ kJ kg}^{-1}$, $\Delta S_{II \rightarrow I} = 102 \pm 3 \text{ J K}^{-1} \text{ kg}^{-1}$ and $\Delta S_{I \rightarrow II} = 104 \pm 3 \text{ J K}^{-1} \text{ kg}^{-1}$.

For the two compounds under study, sources for these very large entropy changes $\Delta S_{II \rightarrow I}$ can be found in the configurational entropy change ΔS^c associated with the release of molecular orientational degrees of freedom and in lattice strain at the transition. The latter can be decomposed in a volumic entropy change ΔS^V associated with the huge expansion occurring across the transition, and in a nonvolumic strain entropy change. The latter cannot be calculated due to the lack of data on temperature-dependent elastic constants (which are difficult to measure due to the brittleness of the compounds) and the reconstructive nature of the transition, but it is expected to be small [12]. Therefore, the nonvolumic strain contribution to the total entropy change will be negligible compared to the volume contribution and thus not be considered in the following discussion.

On the one hand, the configurational entropy change can be calculated from the ratio between the number of accessible configurations in the high- and low-temperature phases (N_I and N_{II} , respectively) as $\Delta S^c = RM^{-1} \ln \left(\frac{N_I}{N_{II}} \right)$. For the two compounds, the tetrahedral molecular symmetry along with the lattice symmetry in the plastic phase enables 2 and 8 nonequivalent orientations associated with the point group T_d and subgroup C_{3v} , respectively. Then, taking into account that there is a single conformation for each compound due to their rigid molecular character, 10 possible configurations are obtained [30]. As for the low-temperature phase, for 1-Cl-ada M phase is completely ordered and therefore $N_{II} = 1$ whereas for 1-Br-ada $N_{II} = 2$ as discussed previously. This yields a configurational entropy change $\Delta S^c = 112.1 \text{ J K}^{-1} \text{ kg}^{-1}$ for 1-Cl-ada and $\Delta S^c = 62.2 \text{ J K}^{-1} \text{ kg}^{-1}$ for 1-Br-ada. On the other hand, the volume entropy change can be estimated as [31]

$$\Delta S^V = \frac{\bar{\alpha}}{\bar{\chi}} \Delta V_{II \rightarrow I} \quad (1)$$

where $\bar{\alpha}$ and $\bar{\chi}$ are the thermal expansion and isothermal compressibility averaged over the two phases close to the transition. For 1-Cl-ada, $\bar{\alpha} = 3.7 \cdot 10^{-4} \text{ K}^{-1}$ and for 1-Br-ada $\bar{\alpha} = 5.9 \cdot 10^{-4} \text{ K}^{-1}$ [15], whereas $\bar{\chi} = 0.31 \text{ GPa}^{-1}$ [32-34] is used for the two compounds. This yields $\Delta S^V \sim 51 \text{ J K}^{-1} \text{ kg}^{-1}$ for 1-Cl-ada and $\Delta S^V \sim 76 \text{ J K}^{-1} \text{ kg}^{-1}$ for 1-Br-ada. Alternatively, assuming a harmonic elastic Helmholtz free energy for the volume change, ΔS^V can also be estimated by using the expression

$$\Delta S^V \simeq \frac{1}{2V} \left\langle \frac{\partial K}{\partial T} \right\rangle \Delta V_{II \rightarrow I}^2 \quad (2)$$

where K is the bulk modulus and the average is taken over the two phases close to the transition. Using $\left\langle \frac{\partial K}{\partial T} \right\rangle \simeq 3.2 \cdot 10^7 \text{ Pa K}^{-1}$ for 1-Cl-Ada calculated from literature data [32], we obtain $\Delta S^V \simeq 44 \text{ J K}^{-1} \text{ kg}^{-1}$ which is in good agreement with the value obtained previously.

While these values are intended to give only a rough estimate (notice that we obtain $\Delta S^c + \Delta S^V > \Delta S_{II \rightarrow I}$), they indicate that for these materials ΔS^V and ΔS^c are of the same order and that vibrational entropy changes at the transition are mainly contributed by volume changes, whereas other contributions are minor. On the other hand, these values are consistent with the suggested trend for adamantane derivatives and observed in some cyclohexanes according to which $\Delta S^c \sim 0.6 \Delta S_{II \rightarrow I}$ [19,35-37]. For 1-Br-ada, the relative

contribution of ΔS^c compared to ΔS^V is minor due to the partial disorder surviving in the O phase. On the other hand, this set of values for ΔS^c and ΔS^V could be also a signature that the orientational disorder in the plastic phase is actually restricted to a smaller number of configurations than the 10 that are nominally achievable for the specific symmetries of these materials. It is worth mentioning here that vibrational entropy changes outside the transition, contributing to changes in the heat capacity (i.e. not associated with the transition latent heat), were analyzed in detail in Ref. [19].

From integration of the calorimetric peaks at high pressures, we obtained that the transition entropy change decreases with pressure for the two compounds (see Fig. 2d,f), which is a behavior observed in other substituted adamantanes [38]. In particular, we obtain $\frac{d|\Delta S_{II \rightarrow I}|}{dp} = -13 \pm 2 \text{ J K}^{-1} \text{ kg}^{-1} \text{ kbar}^{-1}$ and $\frac{d|\Delta S_{I \rightarrow II}|}{dp} = -14 \pm 2 \text{ J K}^{-1} \text{ kg}^{-1} \text{ kbar}^{-1}$ for 1-Cl-ada and $\frac{d|\Delta S_{II \rightarrow I}|}{dp} = \frac{d|\Delta S_{I \rightarrow II}|}{dp} = -14 \pm 2 \text{ J K}^{-1} \text{ kg}^{-1} \text{ kbar}^{-1}$ for 1-Br-ada. Taking into account the decrease of $\Delta S_{II \rightarrow I}$ with pressure and the constant dT/dp in the Clausius-Clapeyron equation, we obtained that the transition volume change also decreases with pressure, which is also a common behavior observed in plastic crystals in general [37,39,40], and in adamantane in particular [26,41].

Endothermic and exothermic transition temperatures, $T_{II \rightarrow I}$ and $T_{I \rightarrow II}$, respectively, were determined from the position of the maximum of the calorimetric peaks. Transition temperatures as a function of pressure are displayed in Fig. 2(c) and (e) for 1-Cl-ada and 1-Br-ada, respectively. The shadowed area indicates the transition peak width, which is narrower for the exothermic transitions because their out of stable equilibrium behavior triggers the transitions abruptly. For 1-Cl-ada, at atmospheric pressure, $T_{II \rightarrow I} = 254 \pm 1 \text{ K}$ and $T_{I \rightarrow II} = 245 \pm 1 \text{ K}$, which renders a hysteresis $\Delta T_{II \rightarrow I} \sim 9 \text{ K}$ that is maintained at high pressure because endothermic and exothermic transition temperatures shift similarly with pressure: $\frac{dT_{II \rightarrow I}}{dp} = 27.4 \pm 0.2 \text{ K kbar}^{-1}$ and $\frac{dT_{I \rightarrow II}}{dp} = 27.0 \pm 0.2 \text{ K kbar}^{-1}$. For 1-Br-ada, at atmospheric pressure, $T_{II \rightarrow I} = 316 \pm 1 \text{ K}$ and $T_{I \rightarrow II} = 308 \pm 1 \text{ K}$, which renders a hysteresis $\Delta T_{II \rightarrow I} \sim 9 \text{ K}$. However, it increases up to $\Delta T_{II \rightarrow I} \sim 12 \text{ K}$ just above atmospheric pressure and increases slightly with pressure because $\frac{dT_{II \rightarrow I}}{dp} = 35.5 \pm 0.5 \text{ K kbar}^{-1} > \frac{dT_{I \rightarrow II}}{dp} = 33.3 \pm 0.8 \text{ K kbar}^{-1}$. From the hysteresis and $\frac{dT_{I \rightarrow II}}{dp}$ we can determine the minimum pressure to achieve reversible BC effects as [12]

$$p_{rev} \simeq \Delta T_{II \rightarrow I} \left(\frac{dT_{I \rightarrow II}}{dp} \right)^{-1}, \quad (3)$$

which yields values as small as ~ 0.3 and $\sim 0.35 \text{ kbar}$ for 1-Cl-ada and 1-Br-ada, respectively. The aforementioned transition thermodynamic data obtained from variable-pressure calorimetry are summarized in Table 1.

3.2 Determination of pressure- and temperature-dependent entropy

Temperature- and pressure-dependent entropy $S(T, p)$ is constructed with respect to a reference entropy $S_0 \equiv S(T_0, p_{atm})$ where T_0 is a reference temperature chosen below but close to the transition temperature at atmospheric pressure. In particular, T_0 is set to 290 K for 1-Br-ada and 220 K for 1-Cl-ada. At T_0 , $S(T_0, p)$ is determined as

$$S(T_0, p) - S(T_0, p_{atm}) = - \int_{p_{atm}}^p \left(\frac{\partial V_{II}}{\partial T} \right)_p dp \simeq - \left(\frac{\partial V_{II}}{\partial T} \right)_{p_{atm}} \Delta p, \quad (4)$$

where we have assumed that $\left(\frac{\partial V_{II}}{\partial T} \right)_p \simeq \left(\frac{\partial V_{II}}{\partial T} \right)_{p_{atm}}$ in the narrow pressure range under study (for 1-Cl-ada $\left(\frac{\partial V_{II}}{\partial T} \right)_{p_{atm}} = (1.83 \pm 0.04) \cdot 10^{-7} \text{ m}^3 \text{ K}^{-1} \text{ kg}^{-1}$ and for 1-Br-ada $\left(\frac{\partial V_{II}}{\partial T} \right)_{p_{atm}} = (2.63 \pm 0.04) \text{ m}^3 \text{ K}^{-1} \text{ kg}^{-1}$ are taken from literature [16]). This assumption is reasonable given the data provided by similar compounds in Ref. [39]. Notice that this procedure corresponds to an indirect method [4] of calculation of BC effects at $T = T_0$.

Above T_0 , $S(T, p) - S(T_0, p)$ is calculated following the quasi-direct method, using our measured variable-pressure isobaric heat flow across the temperature-induced transition and heat capacity data $C_p(T, p_{atm})$ at atmospheric pressure from literature (ref. [42] for 1-Cl-ada and Ref. [19] for 1-Br-ada) for the involved phases. Mathematical details can be found elsewhere [10] and entail that outside the transition regions, $C_p(T, p) \simeq C_p(T, p_{atm})$ within the narrow pressure range under study. Notice that this relation is valid to a very good approximation because the linear dependence of volume on temperature for both 1-Br-ada and 1-Cl-ada relatively close to the transition [15] entails that $C_p(T, p)$ is independent of pressure due to the thermodynamic relation

$$\left(\frac{\partial C_p}{\partial p} \right)_T = -T \left(\frac{\partial V^2}{\partial^2 T} \right)_p = 0. \quad (5)$$

This is further supported by pressure-dependent measurements of heat capacity for adamantane [43], which shows that for this compound C_p is approximately independent or very weakly dependent on pressure in the pressure range under study. It is worth mentioning here that the linear $V - T$ behavior is commonly observed among organic crystals [35].

To combine the pressure independence of C_p with the temperature shift of the transition temperature with pressure, C_p of phase II is extrapolated towards the pressure-dependent transition temperature $T(p)$. The resulting $S(T, p)_{H,C} - S_0$ functions are shown in Fig. 3, where the subscripts H and C stand for curves obtained on heating and on cooling, respectively.

Once the entropy curves are determined, we can obtain insight about their reliability by using two different methods to calculate the isothermal difference between the entropy curves at different pressures at the high temperature phase, $S(T, p) - S(T, p_{atm})$, and compare the obtained results. On the one hand, method 1 consists of directly subtracting the curves. On the other hand, method 2 consists of applying the thermodynamic equation used previously to determine $S(T_0, p) - S(T_0, p_{atm})$ but after replacing T_0 by T [$> T_{II \rightarrow I}(p)$] and V_{II} by V_I , so that we can write $S(T, p) - S(T, p_{atm}) = \int_{p_{atm}}^p \left(\frac{\partial V_I}{\partial T} \right)_p dp \simeq \left(\frac{\partial V_I}{\partial T} \right)_{p_{atm}} \Delta p$ (where $\left(\frac{\partial V_I}{\partial T} \right)_{p_{atm}} = (4.43 \pm 0.07) \cdot 10^{-4} \text{ cm}^3 \text{ K}^{-1} \text{ g}^{-1}$ for 1-Cl-ada and $\left(\frac{\partial V_I}{\partial T} \right)_{p_{atm}} = (5.66 \pm 0.09) \cdot 10^{-4} \text{ cm}^3 \text{ K}^{-1} \text{ g}^{-1}$ for 1-Br-ada). For 1-Cl-ada, under ~ 1 kbar (~ 2 kbar), method 1 yields $\sim 46 \text{ J K}^{-1} \text{ kg}^{-1}$ ($\sim 90 \text{ J K}^{-1} \text{ kg}^{-1}$) and method 2 yields $\sim 42 \text{ J K}^{-1}$

kg^{-1} ($\sim 99 \text{ J K}^{-1} \text{ kg}^{-1}$). For 1-Br-ada, under ~ 1 kbar (~ 2 kbar), method 1 yields $\sim 58 \text{ J K}^{-1} \text{ kg}^{-1}$ ($\sim 134 \text{ J K}^{-1} \text{ kg}^{-1}$) and method 2 yields $\sim 62 \text{ J K}^{-1} \text{ kg}^{-1}$ ($\sim 153 \text{ J K}^{-1} \text{ kg}^{-1}$). Therefore, we obtain values that are in agreement within a relative error of $\sim 10\%$, which contributes to an error over the total BC entropy changes (see next section) of $\sim 3\%$ at ~ 1 kbar and $\sim 5\text{--}8\%$ at 2 kbar. Notice that, as such, these isothermal entropy changes correspond to the BC effects arising outside the transition in the plastic phase, and confirm that their magnitude is typically very large in plastic crystals [10,12].

3.3 Barocaloric effects and performance

To determine the BC effects, we use the quasi-direct method for which ΔS and ΔT are determined as differences between entropy curves at different pressures following isothermal and adiabatic paths, respectively [4]. Since the compounds under study exhibit positive dT/dp , endothermic transitions occur on heating or decreasing pressure while exothermic transitions occur on both cooling or increasing pressure. This entails that irreversible isothermal entropy changes occurring when changing pressure between atmospheric pressure p_{atm} and a given pressure $p > p_{atm}$, are calculated as

$$\Delta S(T, p \rightarrow p_{atm}) = S_H(T, p_{atm}) - S_H(T, p) \quad (6a)$$

$$\Delta S(T, p_{atm} \rightarrow p) = S_C(T, p) - S_C(T, p_{atm}) \quad (6b)$$

(see Fig. 4a,c for 1-Cl-ada and 1-Br-ada, respectively). In turn, irreversible adiabatic temperature changes are obtained as

$$\Delta T(T_s, p \rightarrow p_{atm}) = T(S_H, p_{atm}) - T_s(S_H, p) \quad (7a)$$

$$\Delta T(T_s, p_{atm} \rightarrow p) = T(S_C, p) - T_s(S_C, p_{atm}), \quad (7b)$$

where ΔT is conveniently plotted as a function of the starting temperature T_s of the compression or decompression process (see Fig. 4b,d for 1-Cl-ada and 1-Br-ada, respectively).

Reversible $\Delta S(T)$ [$\Delta S_{rev}(T)$] are obtained as the overlap between $|\Delta S(T, p_{atm} \rightarrow p)|$ and $|\Delta S(T, p \rightarrow p_{atm})|$ whereas reversible ΔT are obtained as

$$\Delta T_{rev}(T_s, p_{atm} \rightarrow p) = T(S_C, p) - T_s(S_H, p_{atm}) \quad (8a)$$

$$\Delta T_{rev}(T_s, p \rightarrow p_{atm}) = T(S_H, p_{atm}) - T_s(S_C, p). \quad (8b)$$

Results are shown in Fig. 5. Maximum values for irreversible and reversible BC effects are plotted in Fig. 6.

In addition to ΔS and ΔT , we calculate two parameters for comparison between different materials. On the one hand, the refrigerant capacity (RC) (see Figs 6c,g), which gives an estimation of the transferable heat between hot and cold reservoirs and corresponds to the area beneath the ΔS vs. T peaks displayed in Figs 4(a,c) and 5(a,c). On the other hand, the coefficient of refrigerant performance (CRP) is approximately defined for BC materials as

$$CRP = \frac{\Delta S \times \Delta T_{rev}}{\frac{1}{2} p \Delta V} \quad (9)$$

so that it takes into account the work needed to drive the transition (see Figs 6d,h). Finally, for practical applications it is desired that materials undergo giant BC effects when in contact with both hot and cold ends, which entails that such giant BC effects should be obtained in a relatively wide temperature interval spanning the whole cycle. In this respect, Fig. 7 shows the temperature spans where minimum values of BC effects are obtained under a given pressure change.

4. Discussion

As it can be seen in Figs 5-7, our results show that both 1-Cl-ada and 1-Br-ada display outstanding reversible BC effects at moderate pressures, reaching $\sim 150 \text{ J K}^{-1} \text{ kg}^{-1}$ isothermally and $\geq 16 \text{ K}$ adiabatically, over a temperature span of $\sim 10 \text{ K}$ under a pressure change of $\sim 1 \text{ kbar}$. A comparison of ΔS_{rev} and ΔT_{rev} obtained upon a pressure change of $\sim 1 \text{ kbar}$ between different BC materials available in literature (see Fig. 8) reveals that the joint values for the compounds studied in this work outperform any other BC material reported so far [9]. The values obtained in this work compare also favorably to maximum reversible values driven by other fields, that for best MC materials reach about $\sim 10 \text{ J K}^{-1} \text{ kg}^{-1}$ and $\sim 5 \text{ K}$ under 2 T created by permanent magnets, and $\sim 15 \text{ K}$ and $19 \text{ J K}^{-1} \text{ kg}^{-1}$ under 5 T, for best eC materials reach $\sim 32 \text{ K}$ and $\sim 45 \text{ J K}^{-1} \text{ kg}^{-1}$ under 700 MPa and for best EC materials reach $\sim 5 \text{ K}$ and $\sim 6 \text{ J K}^{-1} \text{ kg}^{-1}$ [49,50]. The keys for this excellent behavior can be found in typical thermodynamic transition values for plastic crystals (colossal latent heat and volume change) and a small hysteresis. This lower pressure at which colossal barocaloric effects are obtained compared to other compounds, permits narrower walls for the pressurized chamber, which will facilitate the heat transfer with the environment in a future barocaloric cooling device.

Moreover, the temperature range for 1-Cl-ada is optimal because it can span from $\sim 255 \text{ K}$ to room temperature, which matches the operational temperature range of fridges, freezers and air conditioners for most applications, ranging from household devices to industrial or medical applications, such as the storage of medical drugs and vaccines. Notice also that the $\sim 10 \text{ K}$ of temperature span for colossal entropy changes obtained upon a pressure change of $\sim 1 \text{ kbar}$ (see Fig. 8) can be shifted to high temperatures at will (and therefore brought to room temperature) by displacing the pressure range (i.e. increasing both the lower and upper working pressures) while maintaining the pressure change at $\sim 1 \text{ kbar}$. In this respect, a device operating between variable pressure limits can be conceived, to adapt actively to the temperature of the working body. This feature provides 1-Cl-ada with a key advantage with respect to other plastic crystals such as NPG [10,11] or PG [12], that show colossal BC effects from slightly above room temperature. Nonetheless, 1-Br-ada (as NPG or PG) could be more appropriate for cooling at higher temperatures, such as applications in industry or refrigeration of lithium-ion batteries, that degrade above $\sim 330 \text{ K}$ [51].

1-Cl-ada and 1-Br-ada, as plastic crystals in general, suffer from low thermal conductivities due to orientational disorder [9], which in the case of the plastic phase of adamantane reaches $\sim 0.18 \text{ W m}^{-1} \text{ K}^{-1}$ under normal conditions [43]. Here, several aspects should be pointed out. On the one hand, in the ordered phases and/or higher pressures, the thermal conductivities experience a significant increase [43,52]. On the other hand, powdered materials display lower thermal conductivities than their single crystal counterparts because the free path is shortened due to phonon scattering at the grain

boundary. However, powder can be combined with a small percentage of excellent conducting nanoparticles [53] or embedded in highly conductive porous matrix [54-58] resulting in a composite with notably improved thermal conductivity. Finally, as an added value for technological applications, it must be noted that both compounds under study are of low cost, low toxicity (irritant) and nonhazardous [59,60].

5. Conclusions

In this work we have studied the barocaloric performance of two plastic crystals belonging to the family of adamantane derivatives: 1-bromoadamantane and 1-chloroadamantane. In the two cases, the combination of high orientational molecular disordering, very large volume changes across a phase transition and a small to moderate hysteresis allow colossal isothermal entropy changes and giant adiabatic temperature changes upon cyclic application and removal of moderate pressures. Interestingly, colossal BC effects in 1-chloroadamantane span from below to room temperature, making it very suitable for real applications. These materials are outstanding among barocaloric systems and should stimulate similar studies in other adamantane derivatives. Structure refinement of the orthorhombic phase of 1-bromoadamantane has confirmed the uniaxial (around the C_{3v} molecular axis) disorder in this phase.

Acknowledgements

This work was supported by the MINECO projects FIS2017-82625-P and MAT2016-75823-R (Spain), the DGU project 2017SGR-42 (Catalonia), the UK EPSRC grant EP/M003752/1, and the ERC Starting grant no. 680032. X. M. is grateful for support from the Royal Society.

Data Availability

The data that support the findings of this study are available from the corresponding author upon reasonable request.

References

- [1] <https://www.birmingham.ac.uk/Documents/college-eps/energy/Publications/2018-clean-cold-report.pdf>, (accessed November 2019).
- [2] Energy savings potential and rd&d opportunities for non-vapor-compression hvac technologies, <https://www.energy.gov/sites/prod/files/2014/03/f12/Non-Vapor%20Compression%20HVAC%20Report.pdf>, (accessed July 2019).
- [3] L. Mañosa, A. Planes, and M. Acet, *J. Mater. Chem. A* 1 (2013) 4925, doi: 10.1039/C3TA01289A
- [4] X. Moya, S. Kar-Narayan, and N. D. Mathur, *Nat. Mater* 13 (2014) 439, doi: 10.1038/nmat3951.
- [5] C. Aprea, A. Greco, A. Maiorino, C. Masselli, *Int. J. Heat Technol.* 36 (2018) 1155, doi: 10.18280/ijht.360401

- [6] C. Aprea, A. Greco, A. Maiorino, C. Masselli, *Int. J. Refrig.* 109 (2020) 1, doi: 10.1016/j.ijrefrig.2019.09.011
- [7] A. Kitanovski, U. Plaznik, U. Tomc, A. Poredoš, *Int. J. Refrig.* 57 (2015) 288, doi: 10.1016/j.ijrefrig.2015.06.008
- [8] C. Aprea, A. Greco, A. Maiorino, C. Masselli, *Energy*, 190 (2020) 116404, doi: 10.1016/j.energy.2019.116404
- [9] P. Lloveras and J.-L. Tamarit, *Advances and obstacles in pressure-driven solid-state cooling: A review of barocaloric materials*, *MRS Energy & Sustainability*
- [10] P. Lloveras, A. Aznar, M. Barrio, P. Negrier, C. Popescu, A. Planes, L. Mañosa, E. Stern-Taulats, A. Avramenko, N. D. Mathur, X. Moya, and J.-L. Tamarit, *Nat. Commun.* 10 (2019) 1803, doi: 10.1038/s41467-019-09730-9
- [11] B. Li, Y. Kawakita, S. Ohira-Kawamura, T. Sugahara, H. Wang, J. Wang, Y. Chen, S. I. Kawaguchi, S. Kawaguchi, K. Ohara, K. Li, D. Yu, R. Mole, T. Hattori, T. Kikuchi, S.-I. Yano, Z. Zhang, Z. Zhang, W. Ren, S. Lin, O. Sakata, K. Nakajima, and Z. Zhang, *Nature* 567 (2019) 506, doi: 10.1038/s41586-019-1042-5.
- [12] A. Aznar, P. Lloveras, M. Barrio, P. Negrier, A. Planes, L. Mañosa, N. D. Mathur, X. Moya, and J.-L. Tamarit, *J. Mater. Chem. A* 8 (2020) 639, doi: 10.1039/C9TA10947A..
- [13] F. B. Li, M. Li, X. Xu, Z. C. Yang, H. Xu, C. K. Jia, K. Li, J. He, B. Li, H. Wang, *Nat. Commun.* 11 (2020) 4190, doi: 10.1038/s41467-020-18043-1.
- [14] J. Li, D. Dunstan, X. Lou, A. Planes, L. Mañosa, M. Barrio, J.-L. Tamarit, and P. Lloveras, *J. Mater. Chem. A* 20354-20362 (2020), doi: 10.1039/D0TA05399F.
- [15] M. Barrio, R. Levit, P. Lloveras, A. Aznar, P. Negrier, D. Mondieig, and J.-L. Tamarit, *Fluid Phase Equilib.* 459 (2018) 219, doi: 10.1016/j.fluid.2017.07.020.
- [16] L. Wanka, K. Iqbal, and P. R. Schreiner, *Chem. Rev.* 113 (2013) 3516, doi: 10.1021/cr100264t.
- [17] R. Marchenko and A. Potapov, *Molbank* 2017 (2017) M968, doi: 10.3390/M968.
- [18] R. Betz, P. Klüfers, and P. Mayer, *Acta Cryst. E* 65 (2009) o101, doi: 10.1107/S1600536808038452
- [19] A. Bazyleva, A. Blokhin, G. J. Kabo, A. G. Kabo, and Y. U. Paulechka, *J. Chem. Thermodyn.* 37 (2005) 643-647, doi: 10.1016/j.jct.2004.10.005
- [20] Ms modeling (materials studio), version 5.5. <http://www.accelrys.com>.
- [21] J. P. Amoureux and M. Bee, *Acta Cryst. B* 36 (1980), 2636, doi: 10.1107/S0567740880009582.
- [22] M. Foulon and C. Gors, *Acta Cryst. B* 44 (1988), 156, doi: 10.1107/S0108768187010140.
- [23] M. Foulon, T. Belgrand, C. Gors, and M. More, *Acta Cryst. B* 45 (1989), 404, doi: 10.1107/S0108768189002739.
- [24] J. P. Amoureux, M. Bee, and J. L. Sauvajol, *Acta Cryst. B* 38 (1982), 1984, doi: 10.1107/S0567740882007729.
- [25] B. B. Hassine, P. Negrier, M. Barrio, D. Mondieig, S. Massip, and J. L. Tamarit, *Cryst. Growth Des.* 15 (2015), 4149, doi: 10.1021/acs.cgd.5b00764.
- [26] P. Negrier, M. Barrio, J. L. Tamarit, and D. Mondieig, *J. Phys. Chem. B* 118 32 (2014), 9595, doi: 10.1021/jp505280d.
- [27] P. Negrier, B. Ben Hassine, M. Barrio, M. Romanini, D. Mondieig, and J.-L. Tamarit, *Cryst. Eng. Comm.* 22 (2020), 1230, doi: 10.1039/C9CE01910C.
- [28] H. M. Rietveld, *J. Appl. Cryst.* 2 (1969), 65, doi: 10.1107/S0021889869006558.
- [29] H. Toraya and F. Marumo, *Mineral. J.* 10 (1981), 211, doi: 10.2465/minerj.10.211.
- [30] G. B. Guthrie and J. P. McCullough, *J. Phys. Chem. Solids* 18 (1961) 53, doi: 10.1016/0022-3697(61)90083-X.

- [31] A. W. Lawson, *J. Phys. Chem. Solids* 3 (1957) 250, doi: 10.1016/0022-3697(57)90029-X.
- [32] E. L. Gromnitskaya, I. V. Danilov, and V. Brazhkin, *Phys. Chem. Chem. Phys.* 23 (2021) 2349-2354, doi: 10.1039/D0CP04550K.
- [33] J. R. Drabble and A. H. M. Husain, *J. Phys. C* 13 (1980) 1377, doi: 10.1088/0022-3719/13/8/008
- [34] J. Damien, *Solid State Commun.* 16 (1975) 1271-1277, doi: 10.1016/0038-1098(75)90163-5
- [35] G. J. Kabo, A. A. Kozyro, M. Frenkel, and A. V. Blokhin, *Mol. Cryst. Liq. Cryst.* 326 (1999), 333-355, doi: 10.1080/10587259908025424.
- [36] G. Kabo, A. Blokhin, M. Charapennikau, A. Kabo, and V. Sevruck, *Thermochim. Acta* 345 (2000) 125, doi: 10.1016/S0040-6031(99)00393-7.
- [37] M. Jenau and A. Würfänger, *Z. Phys. Chem.* 199 (1997) 255, doi: 10.1524/zpch.1997.199.Part_2.255.
- [38] K. Hara, Y. Katou, and J. Osugi, *Bull. Chem. Soc. Jpn.* 54 (1981) 687, doi: 10.1246/bcsj.54.687.
- [39] A. Aznar, P. Lloveras, M. Barrio, and J. L. Tamarit, *Eur. Phys. J. Special Topics* 226 (2017), 1017-1029, doi: 10.1140/epjst/e2016-60315-4.
- [40] M. Jenau, J. Reuter, J.-L. Tamarit, and A. Würfänger, *J. Chem. Soc. Faraday Trans.* 92 (1996), 1899-1904, doi: 10.1039/FT9969201899.
- [41] C. W. F. T. Pistorius and H. A. Resing, *Molec. Cryst.* 5 (1969) 353, doi: 10.1080/15421406908082943.
- [42] K. Kobashi, T. Kyômen, and M. Oguni, *J. Phys. Chem. Solids* 59 (1998) 667, doi: 10.1016/S0022-3697(97)00226-6.
- [43] J. Wigren and P. Andersson, *Mol. Cryst. Liq. Cryst.* 59 (1980) 137, doi: 10.1080/00268948008073505.
- [44] J. M. Bermúdez-García, M. Sánchez-Andújar, S. Castro-García, J. López-Beceiro, R. Artiaga, and M. A. Senarís-Rodríguez, *Nat. Commun.* 8 (2017) 15715, doi: 10.1038/ncomms15715.
- [45] J. Salgado-Beceiro, A. Nonato, R. X. Silva, A. García-Fernández, M. Sánchez-Andújar, S. Castro-García, E. Stern-Taulats, M. A. Señarís-Rodríguez, X. Moya, and J. M. Bermúdez-García, *Mater. Adv.* 1 (2020) 3167, doi: 10.1039/D0MA00652A.
- [46] A. Aznar, P. Lloveras, J.-Y. Kim, E. Stern-Taulats, M. Barrio, J. L. Tamarit, C. F. Sánchez-Valdés, J. L. Sánchez Llamazares, N. D. Mathur, and X. Moya, *Adv. Mater.* 31 (2019) 1903577, doi: 10.1002/adma.201903577
- [47] P. Lloveras, T. Samanta, M. Barrio, I. Dubenko, N. Ali, J.-L. Tamarit, and S. Stadler, *APL Mater.* 7 (2019) 061106, doi: 10.1063/1.509795.
- [48] A. Aznar, A. Gràcia-Condal, A. Planes, P. Lloveras, M. Barrio, J.-L. Tamarit, W. Xiong, D. Cong, C. Popescu, and L. Mañosa, *Phys. Rev. Mater.* 3 (2019) 044406, doi: 10.1103/PhysRevMaterials.3.044406.
- [49] D. Cong, W. Xiong, A. Planes, Y. Ren, L. Mañosa, P. Cao, Z. Nie, X. Sun, Z. Yang, X. Hong, Y. Wang, *Phys. Rev. Lett.* 122 (2019) 255703, doi: 10.1103/PhysRevLett.122.255703
- [50] L. Mañosa, A. Planes, *Appl. Phys. Lett.* 116 (2020) 050501, doi: 10.1063/1.5140555
- [51] S. Ma, M. Jiang, P. Tao, C. Song, J. Wu, J. Wang, T. Deng, and W. Shang, *Prog. Nat. Sci.* 28 (2018), 653, doi: 10.1016/j.pnsc.2018.11.002.
- [52] D. Szewczyk, A. Jeżowski, G. A. Vdovichenko, A. I. Krivchikov, F. J. Bermejo, J. L. Tamarit, L. C. Pardo, and J. W. Taylor, *J. Phys. Chem. B* 119 (2015), 8468, doi: 10.1021/acs.jpcc.5b04240.

- [53] B. Praveen and S. Suresh, *Eng. Sci. Technol. Int. J.* 21 (2018), 1086, doi: 10.1016/j.jestch.2018.07.010.
- [54] O. Mesalhy, K. Lafdi, A. Elgafy, and K. Bowman, *Energy Convers. and Manag.* 46 (2005), 847, doi: 10.1016/j.enconman.2004.06.010.
- [55] E.-S. Lee, S.-M. Lee, D. J. Shanefield, and W. R. Cannon, *J. Am. Ceram. Soc.* 91 (2008), 1169, doi: 10.1111/j.1551-2916.2008.02247.x
- [56] A. I. Krivchikov, O. A. Korolyuk, I. V. Sharapova, J. L. Tamarit, F. J. Bermejo, L. C. Pardo, M. Rovira-Esteva, M. D. Ruiz-Martin, A. Jezowski, J. Baran, and N. A. Davydova, *Phys. Rev. B* 85 (2012), 014206, doi: 10.1103/PhysRevB.85.014206.
- [57] G. A. Vdovichenko, A. I. Krivchikov, O. A. Korolyuk, J. L. Tamarit, L. C. Pardo, M. Rovira-Esteva, F. J. Bermejo, M. Hassaine, and M. A. Ramos, *J. Chem. Phys.* 143 (2015) 084510, doi: 10.1063/1.4929530
- [58] A. Krivchikov, G. Vdovichenko, O. Korolyuk, F. Bermejo, L. Pardo, J. L. Tamarit, A. Jezowski, and D. Szewczyk, *J. Non-Cryst. Solids* 407 (2015), 141, doi: 10.1016/j.jnoncrysol.2014.08.006
- [59] https://aksci.com/item_detail.php?cat=K331, (accessed October 2020).
- [60] https://aksci.com/item_detail.php?cat=K701, (accessed October 2020).

Table 1. Transition thermodynamic properties at variable pressure.

| | $T_t(p_{atm})$ | | dT/dp | | $\Delta H_t(p_{atm})$ | | $\Delta S_t(p_{atm})$ | | $d\Delta S_t/dp$ | |
|----------|--------------------|--------------------|----------------------|--------------------|-----------------------|--------------------|------------------------------------|--------------------|---|--------------------|
| | K | | K kbar ⁻¹ | | J g ⁻¹ | | J K ⁻¹ kg ⁻¹ | | J K ⁻¹ kg ⁻¹ kbar ⁻¹ | |
| | $II \rightarrow I$ | $I \rightarrow II$ | $II \rightarrow I$ | $I \rightarrow II$ | $II \rightarrow I$ | $I \rightarrow II$ | $II \rightarrow I$ | $I \rightarrow II$ | $II \rightarrow I$ | $I \rightarrow II$ |
| 1-Cl-ada | 254 ± 1 | 245 ± 1 | 27.4 ± 0.2 | 27.0 ± 0.2 | 32.0 ± 1.0 | 31.5 ± 1.0 | 132 ± 4 | 136 ± 4 | -13 ± 2 | -14 ± 2 |
| 1-Br-ada | 316 ± 1 | 308 ± 1 | 35.5 ± 0.5 | 33.3 ± 0.8 | 32.0 ± 1.0 | 31.0 ± 1.0 | 102 ± 3 | 104 ± 3 | -14 ± 2 | -14 ± 2 |

Figure1. (a) X-ray diffraction pattern taken at $T = 295$ K of the orthorhombic phase in 1-Br-ada. The inset shows an enlargement of the 2θ range $(50,80)^\circ$. Red symbols, blue and black lines stand for experimental data, refined pattern and the corresponding difference, respectively. Green symbols indicate the position of Bragg peaks. (b,c) Orthorhombic unit cell of 1-Br-Ada, projected onto (b) the (010) and (c) the (100) planes. Red, gray and white stands for Br, C and H atoms, respectively. Degenerated positions indicate occupational disorder.

Figure2. (a,b) Pressure-dependent calorimetry measurements for (a) 1-Cl-ada and (b) 1-Br-ada. (c,e) Temperature-pressure phase diagram and (d,b) transition entropy change for the two compounds under study. In panels (c-f), red and blue symbols correspond to measurements on heating and cooling, respectively and shadowed areas in (c) and (e) indicate the transition peak width. Lines are linear fits to the data.

Figure3. Isobaric temperature-dependent entropy curves at different pressures obtained on heating (a,c) and on cooling (b,d) for 1-Cl-ada (a,b) and 1-Br-ada (c,d).

Figure 4. (a,c) Isothermal entropy changes and (b,d) adiabatic temperature changes upon first application or removal of pressure BC effects for different applied pressures for (a,b) 1-Cl-ada and (c,d) 1-Br-ada.

Figure 5. Reversible (a,b) entropy and (c,d) temperature changes upon application and removal of pressure under isothermal and adiabatic conditions, respectively, for (a,b) 1-Cl-ada and (c,d) 1-Br-ada.

Figure 6. (a,e) Maximum Isothermal entropy changes and (b,f) adiabatic temperature changes, (c,g) Refrigerant Capacity and (d,h) Coefficient of Refrigerant Performance as a function of pressure changes for (a-d) 1-Cl-ada and (e-h) 1-Br-ada. Red, blue and green data correspond to first compression, first decompression and reversible data. Lines are fits to the data.

Figure 7. Temperature spans where different magnitudes of (a,c) reversible isothermal entropy changes and (b,d) reversible adiabatic temperature changes are obtained, as a function of applied pressure change, for (a,b) 1-Cl-ada and for (c,d) 1-Br-ada.

Figure 8. Comparison between different BC materials: (a) Reversible isothermal entropy changes upon $0 \leftrightarrow \sim 1$ kbar pressure change as a function of temperature. (b) Reversible adiabatic temperature changes upon $0 \rightarrow \sim 1$ kbar pressure increase as a function of temperature. Literature data taken from: PG: [12]; C₆₀: [13]; [TPrA][Mn(dca)₃]: [44]; [(CH₃)₄N]Mn[N₃]₃: [45]; MnCoGeB_{0.03} (asterisk): [46]; (MiNiSi)_{0.60}(FeCoGe)_{0.40} (diamond) and (MiNiSi)_{0.61}(FeCoGe)_{0.39} (triangle): [47]; Ni₅₀Mn_{31.5}Ti_{18.5} (circle): [48].

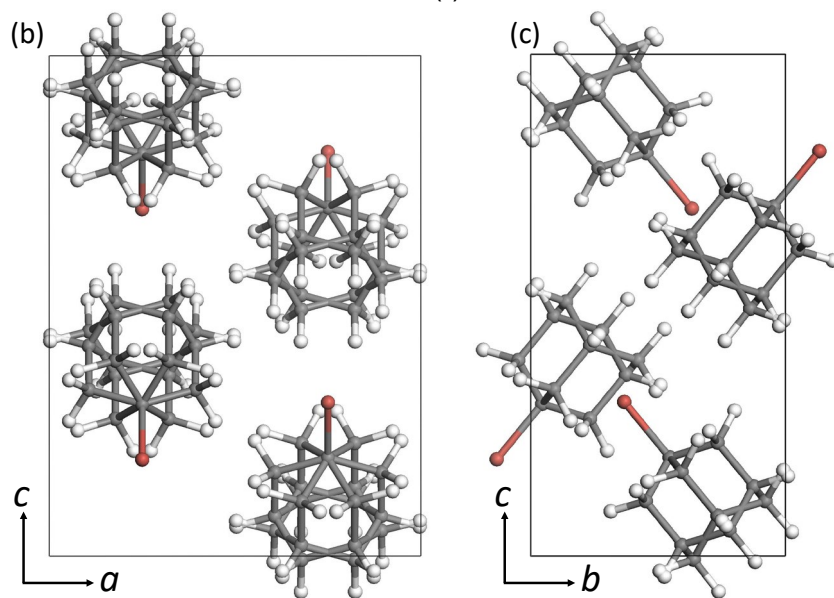
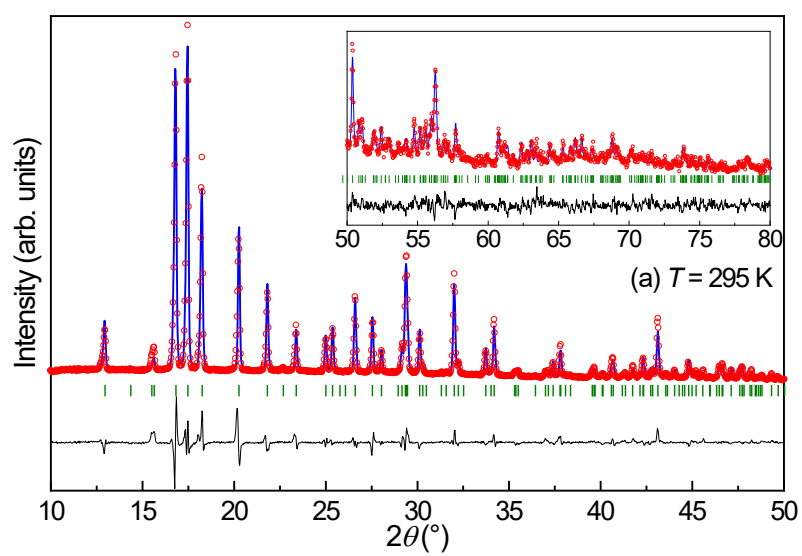


Figure 1

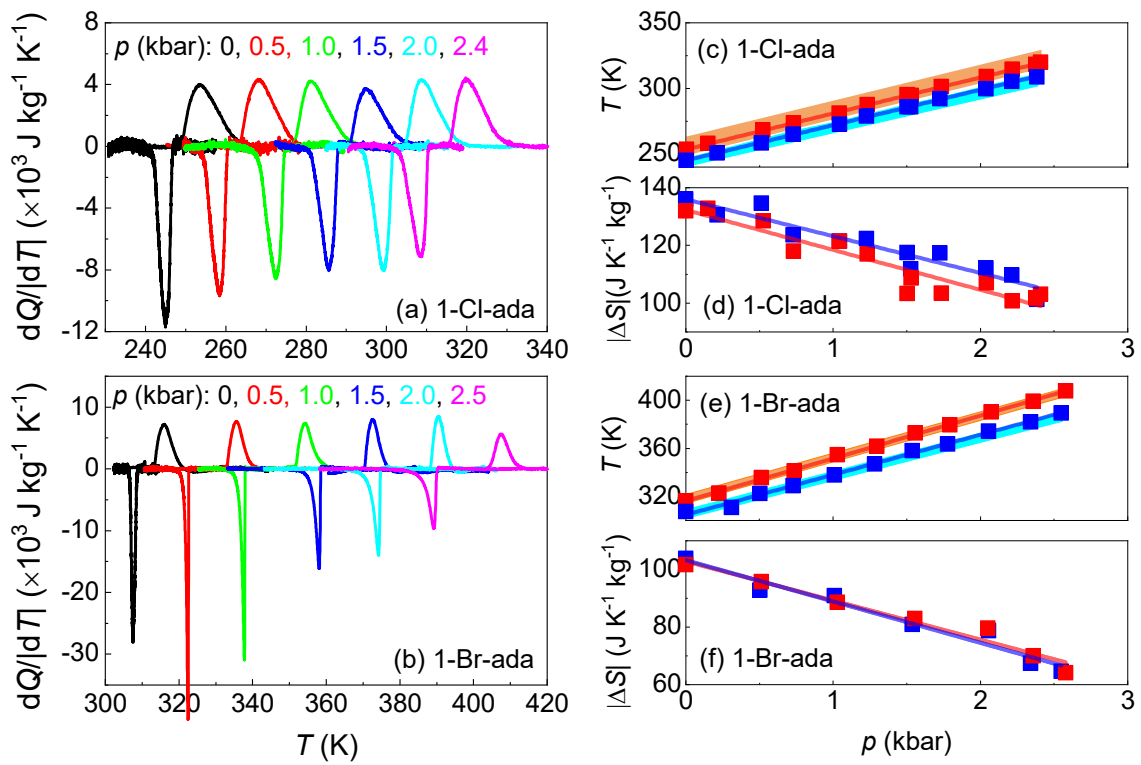


Figure 2

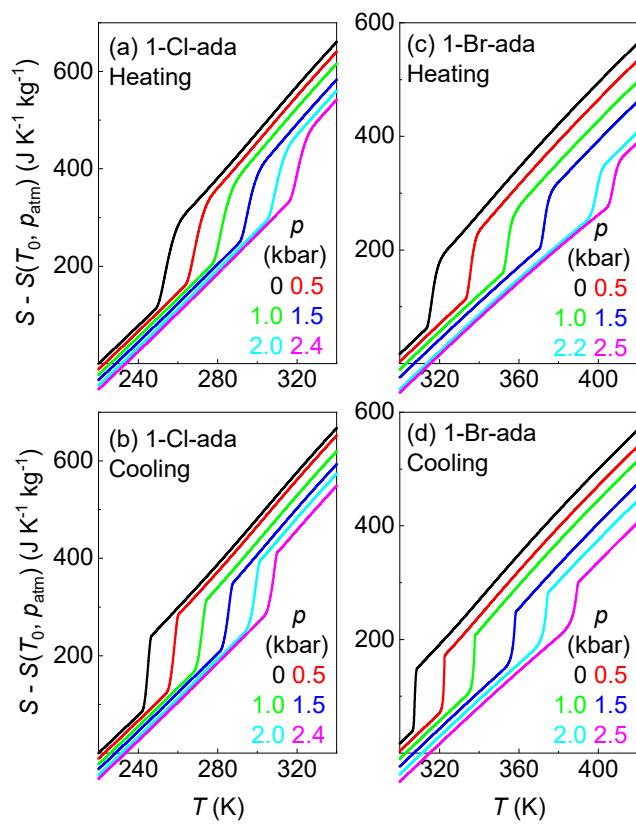


Figure 3

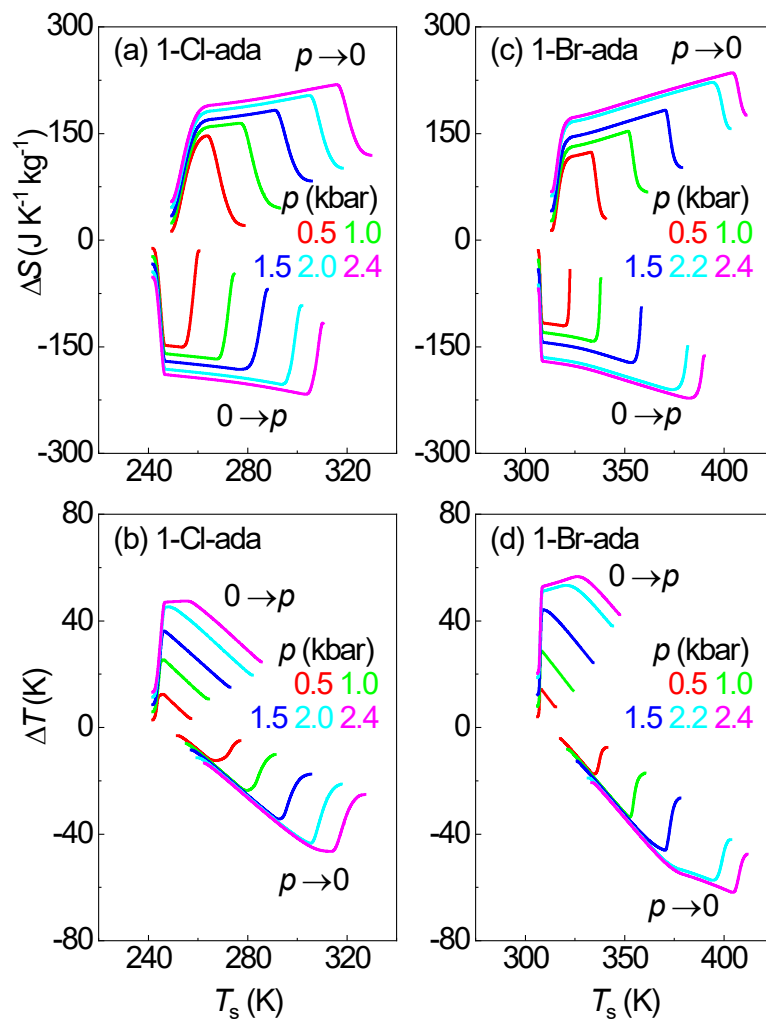


Figure 4

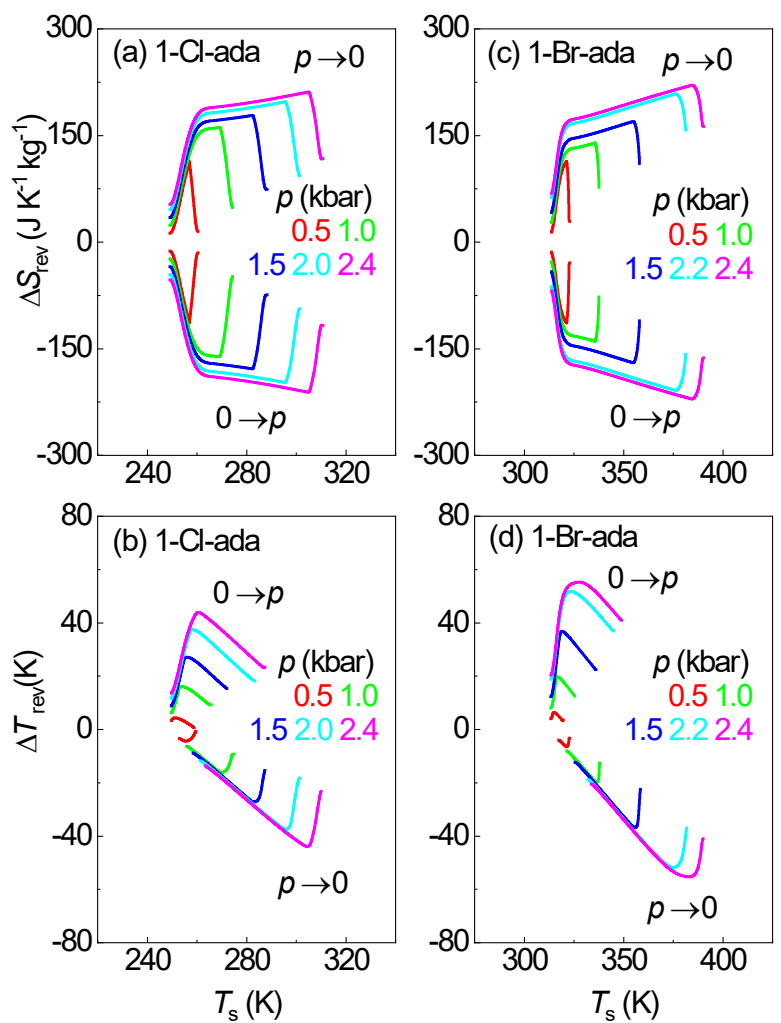


Figure 5

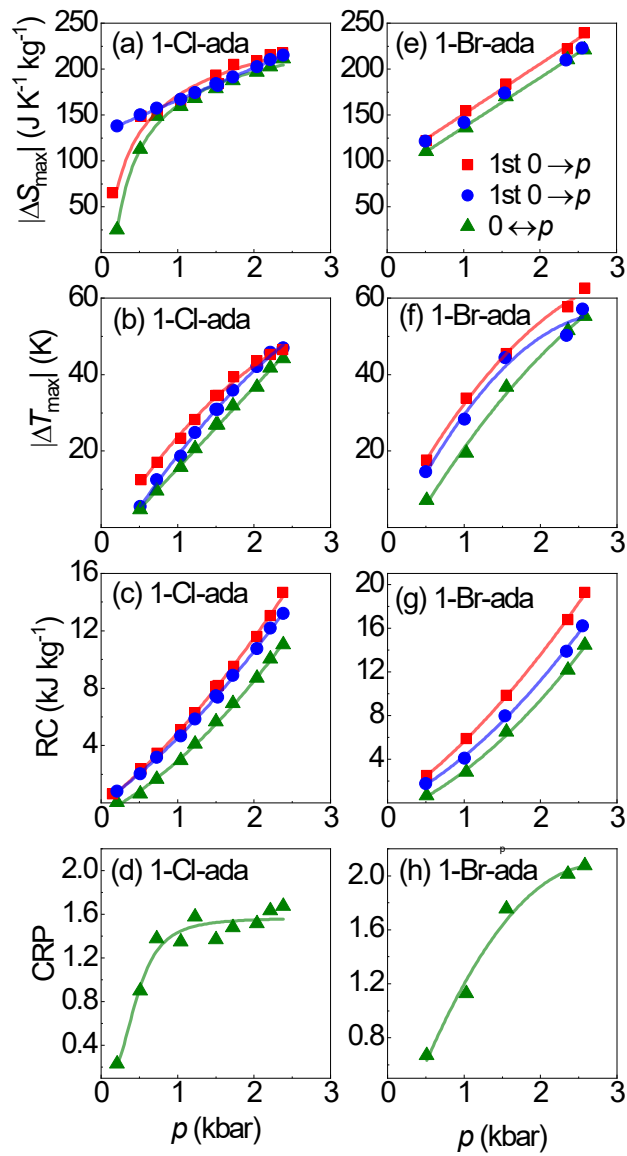


Figure 6

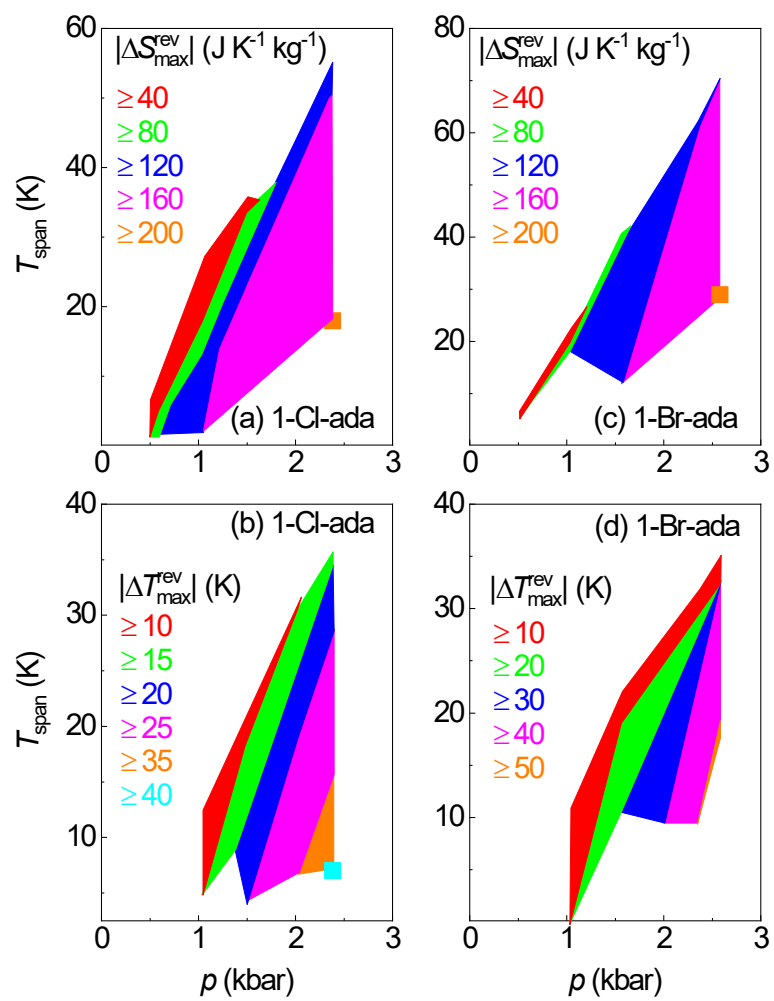


Figure 7

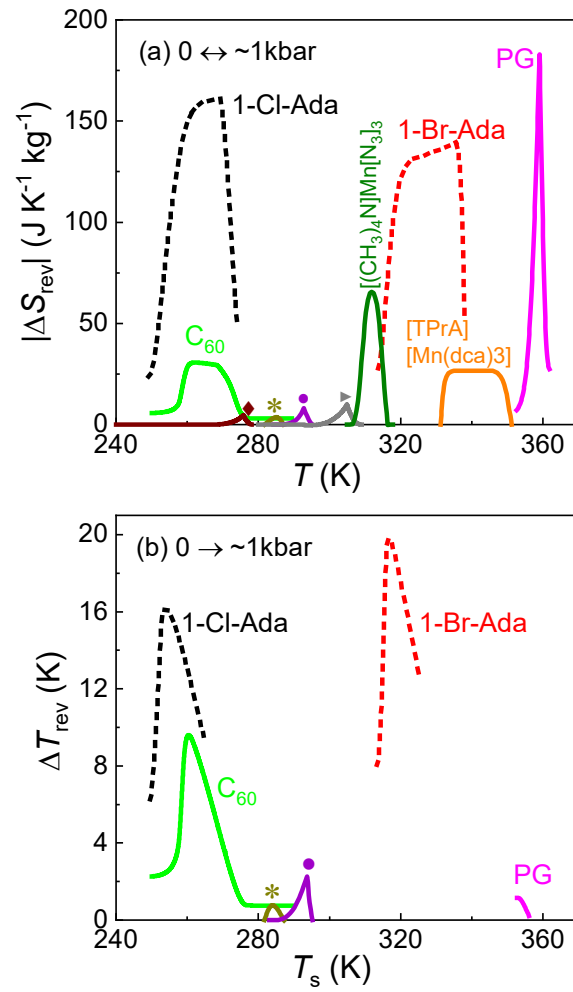


Figure 8